ICARUS 105, 48–66 (1993)

Asteroid Secular Resonant Proper Elements

ALESSANDRO MORBIDELLI

Observatoire de la Côte d'Azur, B.P. 229, 06304 Nice Cedex 4, France

Received January 20, 1993; revised May 10, 1993

A practical algorithm for the computation of the dynamic evolution of asteroids which are inside or close to a secular resonance has been developed. The results are checked with many numerical simulations of both real and fictitious objects. These tests prove that the algorithm is able to identify the dynamic nature of resonant objects and distinguish between future planet crossers and regular bodies. The short CPU time necessary for its execution makes it a useful tool for studying the mechanisms of meteorite transport to the inner Solar System. For this purpose, the sets of initial conditions which lead to large eccentricity in the ν_6 secular resonance are identified. Finally, the dynamic behavior of 44 numbered asteroids very close to the ν_6 resonance is analyzed. Only 4 of these asteroids are found in regions dangerous for their stability. A few others become temporary Mars crossers. The rest of them, as 6 Hebe, have a moderate eccentricity during all their quasi-periodic dynamic evolution.

1. INTRODUCTION

In this paper I present a method for the fast computation of the dynamic evolution of objects of the asteroid belt which are close to a secular resonance and discuss the quality of the results.

It is well known that the theories for the computation of proper elements (see Williams 1969, Milani and Knežević 1990, 1992, Lemaitre and Morbidelli 1992) cannot work in presence of secular resonances. On the other hand, the existing theories on secular resonances (Nakai and Kinoshita 1985, Yoshikawa 1987, Morbidelli and Henrard 1991b) describe, more or less qualitatively, their dynamic properties, but do not provide a direct way to compute for any desired object its secular resonant dynamic evolution.

The scarce interest in the quantitative analysis of secular resonances seems motivated by the fact that actually only a small fraction of real asteroids are near or inside secular resonances; therefore, owing to their limited number, the best way to study the dynamic evolution of these objects is by direct numerical integration. A lot of numerical work has been done in this direction by Froeschlé and Scholl (1987) and Scholl and Froeschlé (1990).

However, the situation changes drastically when one wants to study the dynamics of thousands of fictitious fragments of asteroids, in order to investigate in a statistic way the efficiency of secular resonances in delivering meteorites to the Earth. In a recent paper by Farinella *et al.* (1993), for example, only 18 of thousands of fragments of 6 Hebe were numerically integrated. A numerical integration of 1 Myr takes approximately 10 hr of CPU time on a HP720 machine. Here I propose a semianalytic quantitative method for the computation of the secular evolution of a resonant object as well as for obtaining a picture of the phase space around it that takes less than 1 min of CPU time on the same machine.

The name "resonant proper elements" is somewhat ambiguous and needs to be explained. One can speak of "proper elements" any time one can find an integrable approximation of the problem under study. Now, an isolated secular resonance can be easily approximated by an integrable model. Indeed, secular resonances are not very chaotic: they induce large but regular variations of the eccentricity or the inclination. Chaos exists only close to the critical curve which connects the unstable equilibrium point to itself. It is true that the large variations of the eccentricity often cause the resonant object to become a planet crosser and subsequently have a chaotic motion; however, up to the first close approach, the evolution is deterministic and can be computed with accuracy. Therefore, once an integrable model to approximate the real dynamics has been constructed, one can define a resonant proper element as any identifier of the trajectories of the model. For objects which are in regions of the phase space which are protected from close approaches, one could choose, for example, the values of eccentricity and inclination when the critical angle of the resonance is 0 or 180°. In this paper, however, I prefer to give a picture of the full phase space so that one can easily see the dynamic evolution of the object and understand it by looking at the global resonant topology. Of course, the evolution with respect to time can be provided also.

The algorithm for the computation of the integrable approximation of the resonant dynamics is derived from

0019-1035/93 $5.00

the general theory of secular resonances by Morbidelli and Henrard (1991a) and the theory for the computation of proper elements by Lemaitre and Morbidelli (1992). Its guidelines are explained in Section 2. Briefly put, starting from mean elements (derived from Milani & Knežević's program, see Milani and Knežvič, 1990), instead of eliminating all secular perturbation terms, as in the case of the computation of the usual proper elements, I eliminate only the nonresonant harmonics. What I get is an integrable Hamiltonian $K(J, Z, \sigma)$, where σ is the critical angle of the resonance in study, canonically conjugated to a linear combination of the actions J and Z. Therefore, the computation of the resonant proper elements of an asteroid proceeds in two steps. First I compute its "semiproper elements," i.e., a set of values of the action-angle variables J, Z, σ after the elimination of the nonresonant terms. Second, using the semiproper elements as initial conditions, I compute the secular evolution integrating the resonant Hamiltonian K. Alternatively, I plot the initial conditions onto the picture of the phase space of K, thus getting a global view of the dynamics.

In Section 3 I discuss the results from the real resonant asteroids, the numerical integrations of which are available in the literature. These objects are in the main secular resonances ν_5, ν_6, or ν_{16}. The ν_5 resonance occurs when the precession rate of the asteroid's longitude of perihelion is in 1/1 resonance with the precession rate g_5 of the perihelion of Jupiter; the ν_6 resonance is the 1/1 commensurability with the precession rate g_6 of the perihelion of Saturn; the ν_{16} resonance is the corotation between the nodes of the asteroid and of Jupiter–Saturn (the nodes of Jupiter and Saturn are alligned, i.e., $\Omega_J = 180° + \Omega_5$, in the approximation which neglects the perturbations of the other planets). I will discuss also the connection with the nonresonant proper elements (Lemaitre and Morbidelli, 1992) for those objects which are close to the resonance, like 582 Olympia (close to ν_5) and 739 Mandeville (close to ν_6).

Section 4 is devoted to a deeper investigation of the ν_6 resonance. The phase space associated with this resonance has a peculiar topology, somewhat different from the classical picture provided by the "second fundamental model" (see Henrard and Lemaitre, 1983). This makes this resonance much stronger than the other ones, in the sense that it can pump the eccentricity up to extremely large values (>0.8). The semianalytical results have been tested with many numerical integrations by R. Gonczi, and some comparisons are shown in this paper. In order to have a good correspondence with *all* the numerical results, the frequency of the longitude of perihelion computed for the asteroids has been corrected by 0.4 arcsec/year. This correction is of the same order as the contribution of the inner planets, which are not taken into account in the model.

Moreover, by running the resonant proper elements program for several initial conditions, I carry out a systematic exploration of the ν_6 resonance, which allows me to point out the locations of the regions of danger in the space of mean elements, where the eccentricity is forced to increase up to at least 0.4.

Finally, I examine the behavior of the numbered asteroids which currently have moderate eccentricity and which are very close to the resonance, so that nonresonant proper elements are not convergent or have a poor accuracy. I find that only four of these asteroids are actually in regions dangerous for their stability and should be considered as temporary objects in the main asteroid belt. A few others, although stable from the point of view of resonant dynamics, become temporary Mars crossers. The rest of them, such as 6 Hebe, have a moderate eccentricity during all their quasi-periodic dynamic evolution.

2. THEORETICAL BACKGROUND FOR THE COMPUTATION OF RESONANT PROPER ELEMENTS

This section is devoted to a brief explanation of the algorithm for the computation of the resonant dynamics. Actually, this algorithm is nothing but a modification of the one for the computation of nonresonant proper elements (see Lemaitre and Morbidelli, 1992), so I refer to that paper for a more detailed description and for all common technical details.

In my model, I take into account the perturbation effects of Jupiter and Saturn. The Hamiltonian of the problem is averaged with respect to the mean longitudes of the asteroid and the planets, provided that they are not in a mean motion resonant configuration. The averaging operation introduces, following the Lie algorithm, terms of higher order in the perturbing masses of the planets. Here I take into account only the quadratic term in the mass of Jupiter. The averaged Hamiltonian is computed without any expansion in power series of the eccentricity and the inclination of the asteroid, in order to have an accurate model also for large values of these variables. The Hamiltonian and its derivatives are stocked once for ever in a three-dimensional grid in the a–e–i space as in (Lemaitre and Morbidelli, 1992). By spline interpolation one then computes the Hamiltonian at any desired point of the phase space.

The key point of our theory of secular motion (and of Williams' one, see Williams 1969) is the expansion of the averaged Hamiltonian in power series of the eccentricity and inclination of the planets, which are small and therefore assumed as perturbation parameters. Then, only the linear terms in (e', i') (the $'$ symbol referring to the planets) are retained, consistent with our perturbation approach,

which is a first-order one. With these settings, the secular Hamiltonian K is split into $K_0 + K_1$, where K_0 is the averaged perturbation caused by the planets, assumed to be on coplanar circular orbits, and K_1 is the linear part in (e', i').

It is easy to prove (Kozai 1962) that K_0 is a two-degrees-of-freedom integrable Hamiltonian, although its dynamics are not trivial. In particular, at a critical inclination ($\sim 35°$ in the asteroid belt) the argument of perihelion can librate, while, at lower inclination, the argument of perihelion always circulates. On the other hand, K_1 is time dependent, since it depends on the variables of the planets which are assumed to change with time following the linear theory relationship,

$$
\begin{aligned}
e'_j \cos(\tilde{\omega}'_j) &= M_{j,5} \cos(g_5 t + \lambda_5^0) + M_{j,6} \cos(g_6 t + \lambda_6^0) \\
e'_j \sin(\tilde{\omega}'_j) &= M_{j,5} \sin(g_5 t + \lambda_5^0) + M_{j,6} \sin(g_6 t + \lambda_6^0) \\
\sin i'_j \cos \Omega'_j &= N_{j,6} \cos(s_6 t + \mu_6^0) \\
\sin i'_j \sin \Omega'_j &= N_{j,6} \sin(s_6 t + \mu_6^0)
\end{aligned}
$$

the index j referring to Jupiter ($j = 5$) and Saturn ($j = 6$).

In the following we assume K_1 to be a perturbation of K_0. In order to study this dynamic system, we first introduce suitable canonical Arnold action-angle variables (J, ψ, Z, z) in order to transform K_0 into a Hamiltonian independent of the angles ψ and z. A detailed discussion on these action-angle variables and on the way to handle them numerically can be found in previous papers (Morbidelli and Henrard, 1991a) and (Lemaitre and Morbidelli, 1992). Here I recall only the "meaning" of these variables. Since K_0 is integrable, its phase space is foliated into invariant tori. The values of the actions J and Z identify each torus. Z turns out to be $\sqrt{a}(1 - \sqrt{1 - e^2} \cos i)$, while J is the area (divided by 2π) enclosed by the orbit obtained integrating K_0 in the coordinates $(\sqrt{a(1 - e^2)}(1 - \cos i), \omega)$, where ω is the argument of perihelion. Moreover, the angles ψ and z are linear functions of time; i.e., they have constant frequencies ν_ψ and ν_z (functions of the torus (J, Z)). The frequency ν_ψ is equal to $2\pi/T$, where T is the period of circulation/libration of the argument of perihelion; the frequency ν_z is the average frequency of the longitude of perihelion (with opposite sign).

The action-angle variables (J, ψ, Z, z) are then introduced in the perturbation K_1. Here lies the main difference with respect to our work on nonresonant proper elements (Lemaitre and Morbidelli, 1992): instead of evaluating K_1 in the new variables in closed form, I compute here its Fourier expansion; specifically, I write it in the form

$$
\begin{aligned}
K_1 = &\sum_k c_k^5(J, Z) \cos(k\psi - z - g_5 t - \lambda_5^0) \\
&+ \sum_k c_k^6(J, Z) \cos(k\psi - z - g_6 t - \lambda_6^0) \\
&+ \sum_k d_k^6(J, Z) \cos((k + 1)\psi - z - s_6 t - \mu_6^0),
\end{aligned}
$$

with k running on the set of even integers. The coefficients c_k^5, c_k^6, and d_k^6 can be computed numerically by F.F.T. on each torus (J, Z). Of course, in practice the series must be truncated; the results shown in this paper are obtained by truncating with $|k| < 100$.

The following step is the elimination of the angular terms in K_1. This is done by applying the Lie algorithm, here up to the first order only. In other words, I look for a function W_1 such that

$$
\{W_1, K_0\} + K_1 = 0,
$$

where $\{\ \}$ denotes the Poisson bracket.

The explicit knowledge of the (truncated) Fourier expansion of K_1, allows an explicit computation of W_1, which turns out to be:

$$
\begin{aligned}
W_1 = &\sum_k -\frac{c_k^5(J, Z)}{k\nu_\psi - \nu_z - g_5} \\
&\times \sin(k\psi - z - g_5 t - \lambda_5^0) \\
&+ \sum_k -\frac{c_k^6(J, Z)}{k\nu_\psi - \nu_z - g_6} \\
&\times \sin(k\psi - z - g_6 t - \lambda_6^0) \\
&+ \sum_k -\frac{d_k^6(J, Z)}{(k + 1)\nu_\psi - \nu_z - s_6} \\
&\times \sin((k + 1)\psi - z - s_6 t - \mu_6^0).
\end{aligned} \tag{1}
$$

The advantage of this formulation with respect to that in Lemaitre and Morbidelli (1992), which makes no use of explicit Fourier series expansion, is that the effect of each perturbation term can be analyzed separately. In particular, close to a secular resonance, one of the denominators in (1) becomes small, and the effect of the corresponding term is particularly large.

In the complete nonresonant case (none of the denominators is very small), all angular terms in K_1 can be removed. In this case I obtain a procedure for the computation of nonresonant proper elements which is perfectly equivalent to that in (Lemaitre and Morbidelli, 1992). In short, the function W_1 generates a canonical transformation to new variables $(J, \bar{\psi}, \bar{Z}, \bar{z})$, implicitly defined by

$$
\begin{aligned}
J &= \bar{J} + \frac{\partial W_1}{\partial \psi}(\bar{J}, \bar{\psi}, \bar{Z}, \bar{z}, t) \\
Z &= \bar{Z} + \frac{\partial W_1}{\partial z}(\bar{J}, \bar{\psi}, \bar{Z}, \bar{z}, t) \\
\psi &= \bar{\psi} - \frac{\partial W_1}{\partial J}(\bar{J}, \bar{\psi}, \bar{Z}, \bar{z}, t) \\
z &= \bar{z} - \frac{\partial W_1}{\partial P}(\bar{J}, \bar{\psi}, \bar{Z}, \bar{z}, t).
\end{aligned} \tag{2}
$$

This implicit equation is solved in an iterative way. The new variables $(\bar{J}, \bar{\psi}, \bar{Z}, \bar{z})$ are called *proper action-angle variables*, since they are constant of motion up to the first order in the perturbation parameters (e', i'). They are directly related to the nonresonant *proper elements*. [The limits of definition of the actions (which correspond to $e = 0$ or $i = 0$) are singularities for the solution of (2), which could be eliminated using suitable Cartesian coordinates; the use of the latter, however, gives rise to many difficulties of technical type, so action-angle variables are still preferred].

Let us assume, on the contrary, that we are in presence of one isolated secular resonance (i.e., only one denominator in (1) is very small); in this case the dynamics are much more complex, and one cannot eliminate all the perturbation harmonics at one time. However, one can still define in a perturbative way an integrable model of the dynamics as a useful tool to approximate the real behavior. The perturbation approach is explained in the following.

First I proceed to the elimination of all angular terms in K_1 except the resonant one. Therefore, I look for a function W_1 such that

$$\{W_1, K_0\} + K_1 = \text{resonant term},$$

so that W_1 has the form (1) after dropping the term with the small denominator. The implicit Eq. (2) defines new variables $(\bar{J}, \bar{\psi}, \bar{Z}, \bar{z})$ which I call now *semiproper* action-angle variables, since the resonant term has not been eliminated from K_1. From the practical point of view, I simplify this procedure, by setting in (2) $\psi = \bar{\psi}$ and $z = \bar{z}$; as a matter of fact, the correction of the angles is of order of a couple of degrees only and has a second-order effect on the computation of the semiproper actions. This simplification has the advantage that the derivatives of W_1 (and therefore of K_1) with respect to J and Z are no longer necessary, thus speeding up the execution of the algorithm.

In the semiproper action-angle variables, the new Hamiltonian reads

$$K_0(\bar{J}, \bar{Z}) + \alpha(\bar{J}, \bar{Z}) \cos(k\bar{\psi} - \bar{z} - \nu t - \beta), \tag{3}$$

where α indicates generically one of the coefficients c_k^5, c_k^6, or d_k^6, and (ν, β) one of the pairs (g_5, λ_5^0), (g_6, λ_6^0), or (s_6, μ_6^0), according to the resonance under study. It is easy to see that (3) is the integrable model of the resonance that I am looking for. Indeed, one can introduce new canonical variables,

$$
\begin{aligned}
\sigma &= -k\bar{\psi} + \bar{z} + \nu t + \beta, \quad & S &= \bar{Z} \\
\vartheta &= \bar{\psi}, & \Theta &= k\bar{Z} + \bar{J},
\end{aligned} \tag{4}
$$

so that (3) becomes

$$K_0(S, \Theta) + \nu S + \alpha(S, \Theta) \cos\sigma. \tag{5}$$

The dynamics described by (5) are confined on a surface Θ = constant. The values of the semiproper actions obtained solving (2) define the value of this constant. Therefore, on the surface Θ = constant, I compute for several values of S the functions $K_0(S, \Theta)$ and $\alpha(S, \Theta)$. Actually, I compute $\partial K_0/\partial S$ (which is nothing but $\dot{\sigma}$), and α on 10 points covering the interval of definition of S, and I interpolate by monodimensional cubic splines. The value of K_0 is computed integrating the interpolation function, and $\partial\alpha/\partial S$ by taking the derivative of the interpolation function.

At this point, the integrable model of the secular resonance is completely determined. The last step is the computation of the dynamical evolution of the asteroid. The values of the semiproper action-angle variables obtained solving (2) define the values of S and σ associated to the present state of the asteroid. These are the initial conditions for the integration of the equations of motion given by (5), which describe the evolution $(S(t), \sigma(t))$ over the time t. Equivalently, one can have a global picture of the resonant phase space by simply plotting the level curves of (5) and putting the present position of the asteroid (S, σ) on it. This is what has been done for the test asteroids analyzed in Section 3.

Of course, one is interested in obtaining the dynamic evolution of an asteroid in terms of the usual Keplerian variables instead of the new action-angle variables (S, σ). The conversion from the new variables to the more familiar Keplerian ones is straightforward and is analogous to that discussed in Lemaitre and Morbidelli (1992). Given a pair (S, Θ), by inversion of (4) I compute the semiproper actions $\bar{J}$ and $\bar{Z}$. These identify one orbit of the integrable averaged Hamiltonian K_0, which describes the periodic evolution of the mean values of e and i along with the circulation/libration of the argument of perihelion ω. By choosing a reference value of ω (surface of section) one finally associates to (S, Θ) a pair (e, i).

3. TESTS OF THE RESULTS ON THE BEHAVIOR OF SOME REAL ASTEROIDS

In this section I analyze the numerical integrations of real resonant asteroids which I have found in the literature. The aim is to compare these simulations with the theoretical results of the resonant proper elements algorithm and to show how the latter allows one to recover, in a unitary scheme, all the known numerical results.

The first asteroid I analyze here is 945 Barcelona. This object has been numerically integrated by Scholl and Froeschlé (1990), who found it to be in the ν_5 resonance. The picture on the left of Fig. 1 shows my theoretical result. The coordinates are $x = e\cos\sigma$ and $y = e\sin\sigma$, where σ is the critical angle of the ν_5 resonance; i.e., $\tilde{\omega} - g_5 t - \lambda_5^0$, or, approximately, $\tilde{\omega} - \tilde{\omega}_J$, the subscript J referring to Jupiter. The dot denotes the present position of Barcelona in the semiproper elements space, defined by removing all perturbation terms except the resonant one (see Section 2). The picture provides a global view of the resonant dynamics, the curves denoting the lines of motion. Barcelona is in the banana-shape region of libration.

The two pictures on the right show the results of the numerical integration and are taken from Scholl and Froeschlé paper (1990). The top picture shows the forward integration, the bottom one the backward integration, both on a time scale of 1 Myr. The coordinates are $\psi_1^J = [2(1 - \sqrt{1 - e^2})]^{1/2}\cos(\tilde{\omega} - \tilde{\omega}_J)$ and $\psi_2^J = [2(1 - \sqrt{1 - e^2})]^{1/2}\sin(\tilde{\omega} - \tilde{\omega}_J)$, which are close to my x and y. The numerical integration shows essentially a two-time-scale behavior. The "epicycles" which cause large variations of the eccentricity are associated to the rotation of the argument of perihelion ω, which is the secular motion

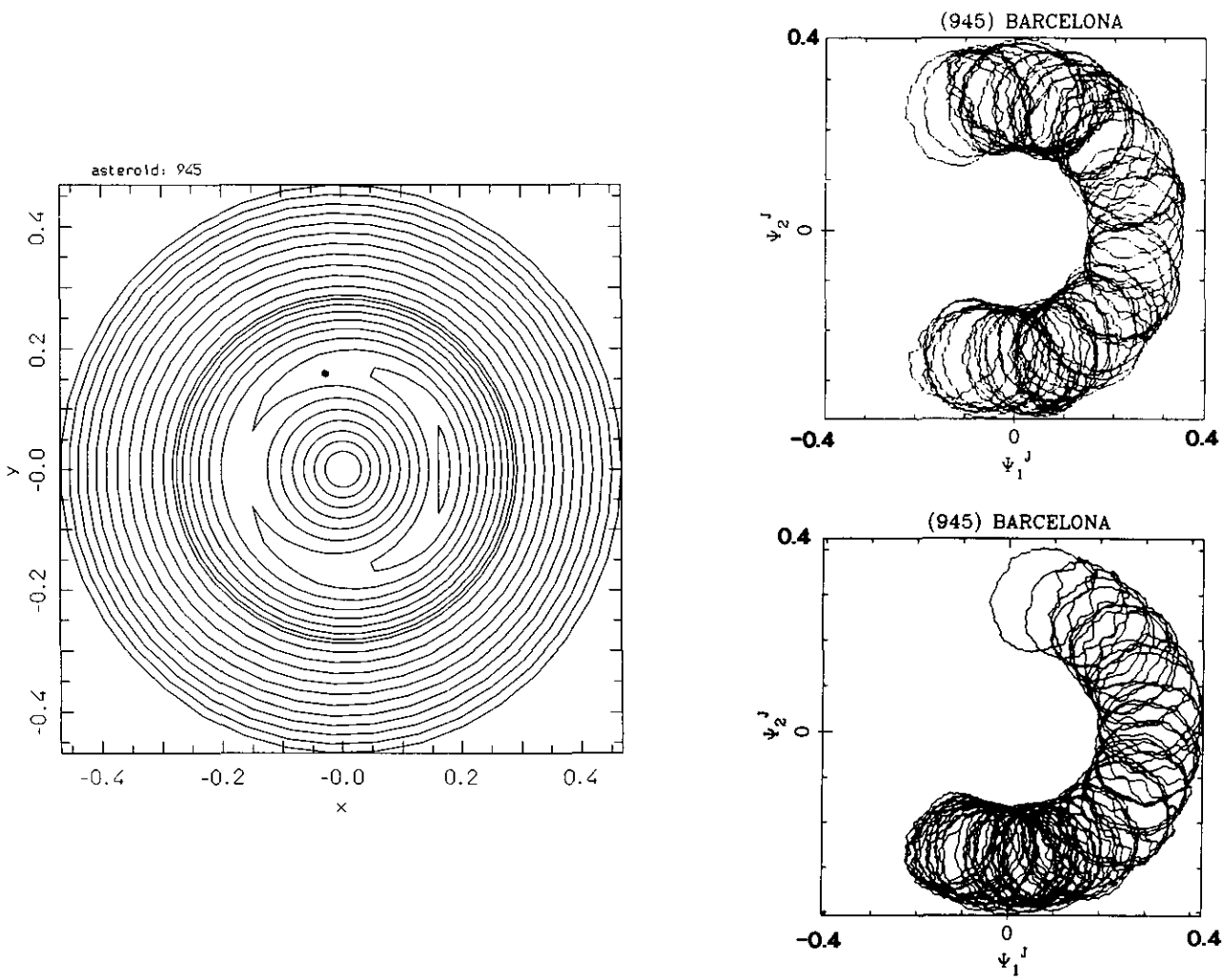

FIG. 1. Asteroid 945 Barcelona in the ν_5 resonance: on the left the results of the theoretical model. On the right the results of the numerical integration. (Top) The forward integration for 1 Myr; (bottom) the backward integration for 1 Myr.

with the shortest time scale. The banana-shape libration is the real dynamical effect of the ν_5 resonance. In order to compare the numerical integration with the theoretical result, one should remember that the theoretical picture shows the resonant motion on the surface of section $\omega = 0$, which corresponds to select the minimal value of the eccentricity on each "epicycle." Therefore, one should compare the inner edge of the banana in the numerical integration with the theoretical curve. Doing so, one sees that in the numerical integration Barcelona cuts the $\psi_2^J = 0$ axis at $e = 0.15$ in the forward integration and $e = 0.20$ in the backward integration. This is in very good agreement with the result of the theoretical model.

The next asteroid I analyze is 582 Olympia. This asteroid is very close to the ν_5 resonance, as the theoretical model shows (Fig. 2, left). The critical angle of the resonance circulates very close to the critical curve which separates librating orbits from circulating ones. The eccentricity (referring again to the section $\omega = 0$) is computed to be equal to 0.10 when $\sigma = \pi$ and 0.18 when $\sigma = 0$. The two pictures on the right of Fig. 2 show the results of the numerical integration, taken again from Scholl and Froeschlé (1990). The top picture concerns the evolution of the critical angle with respect to time, which circulates very slowly; the bottom picture shows the eccentricity as a function of the critical angle, in rectangular coordinates. Again, to compare with the theoretical prediction, one has to look at the minimal eccentricity on each epicycle; the values of the eccentricity when $\tilde{\omega} - \tilde{\omega}_J = 0$ and $\tilde{\omega} - \tilde{\omega}_J = \pi$ (about 0.18 and 0.10, respectively) are again in good agreement with the predictions of the model.

Since 582 Olympia is not inside the secular resonance, but only close to it, it is possible to compute for this

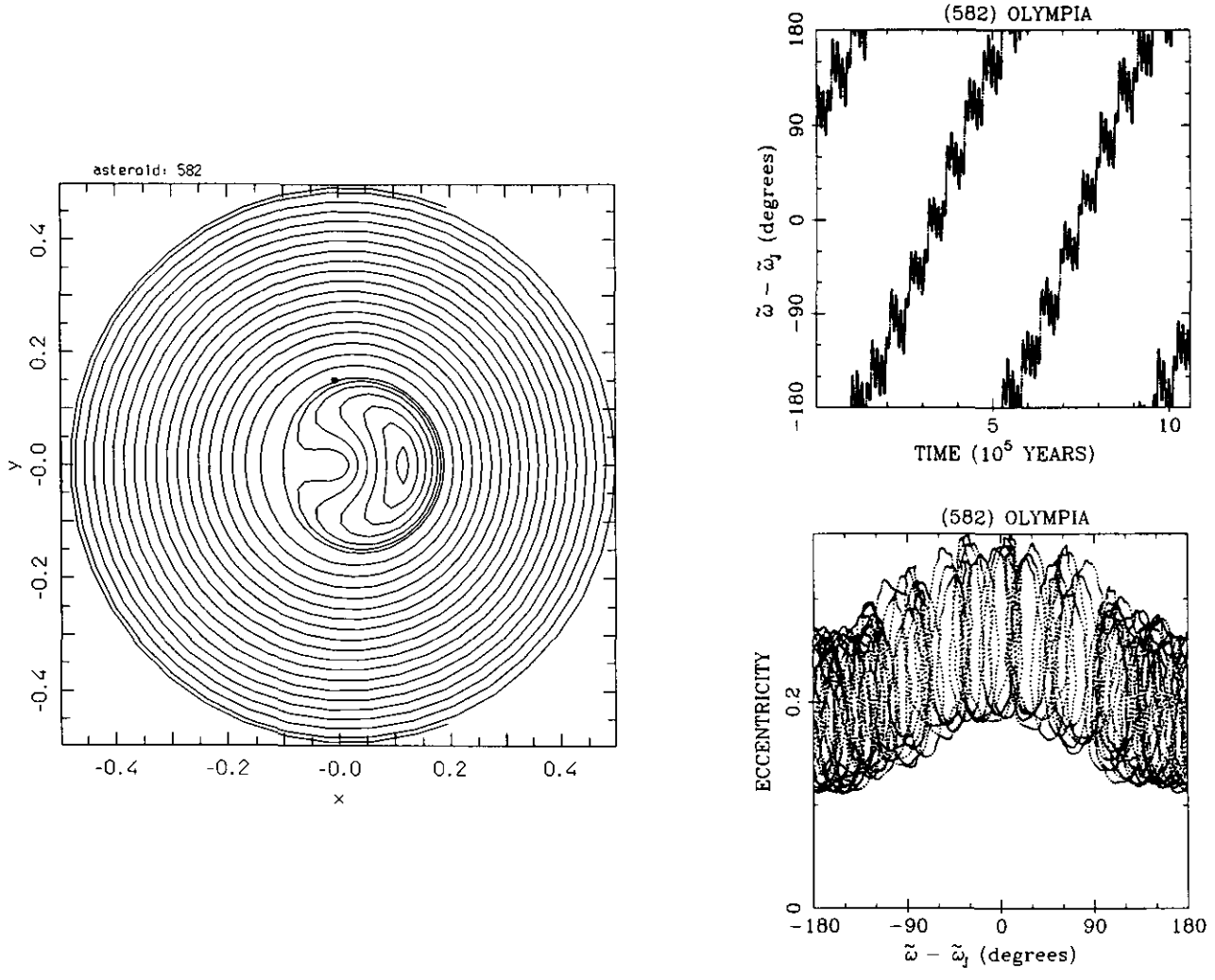

FIG. 2. Asteroid 582 Olympia close to the ν_5 resonance. On the right the phase space given by the theoretical model. On the left the results of the numerical integration.

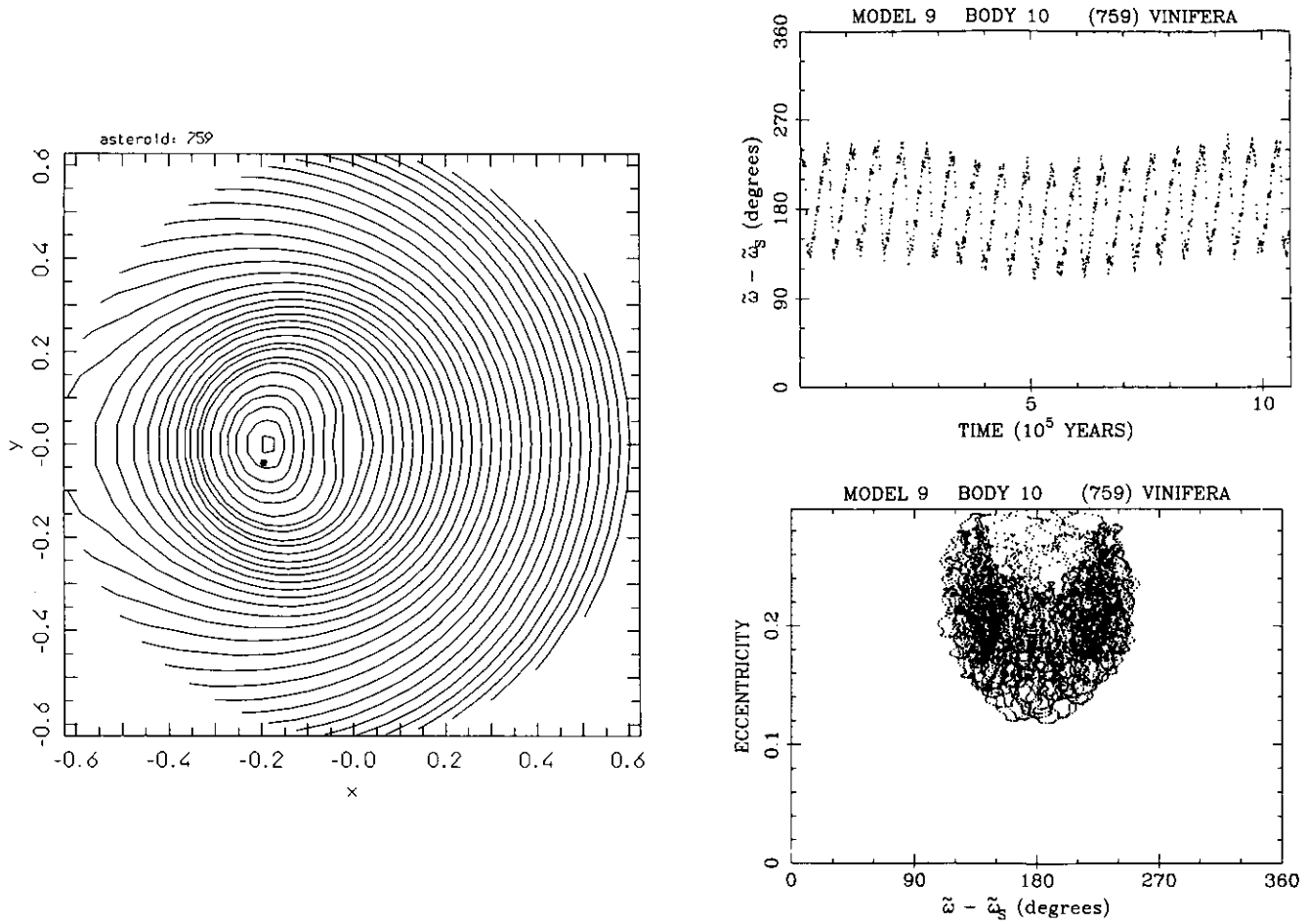

FIG. 3. Asteroid 759 Vinifera in the ν_6 resonance.

asteroid also its nonresonant proper elements. As a matter of fact, in this case the accuracy of nonresonant proper elements is somewhat poor, due to the resonance not being far away. However, apart from these accuracy problems (which causes the nonresonant proper elements to be unsuitable, e.g., for family searches), the connection between resonant and nonresonant proper elements is simple, in principle: the resonant proper elements program gives the evolution of the eccentricity as a function of σ, and, in particular, its minimal and maximal value assumed at $\sigma = \pi$ and $\sigma = 0$; the nonresonant proper elements program gives the average of the eccentricity with respect to the motion of σ. In this case the proper eccentricity is found to be about 0.15.

I come now to analyze some real asteroids which are in the ν_6 secular resonance or close to it.

The first one is 759 Vinifera. In Fig. 3, the picture on the left shows my result. The coordinates x and y are defined with respect to the critical angle of the ν_6 resonance which is $\tilde{\omega} - g_6 t - \lambda_6^0$ (again called σ for simplicity). According to the theoretical model, the critical angle of the resonance librates with very small amplitude around a stable equilibrium point at $\sigma = \pi$. The picture in the upper right corner shows the results of the numerical integration, this time taken from Froeschlé and Scholl (1987). A remark is necessary: the authors plot the evolution of $\tilde{\omega} - \tilde{\omega}_S$ (the subscript S referring to Saturn) instead of the evolution of σ; the difference is $\tilde{\omega}_S - g_6 t$ and is responsible for the oscillations with about 50,000 years period and 50° amplitude which are clearly visible on the plot. Therefore, in order to compare the numerical simulation with the theoretical result, one should mentally average out such oscillations and look at the long periodic oscillation (the period of which is about 1 Myr), which has indeed a small amplitude (some 15°). The picture below shows the evolution of the eccentricity as a function of $\tilde{\omega} - \tilde{\omega}_S$. The average value (about 0.2) is close to that predicted by the theory.

The asteroid 1222 Tina, which has been also integrated in Froeschlé and Scholl (1987), has a very similar dynamic behavior (see Table II).

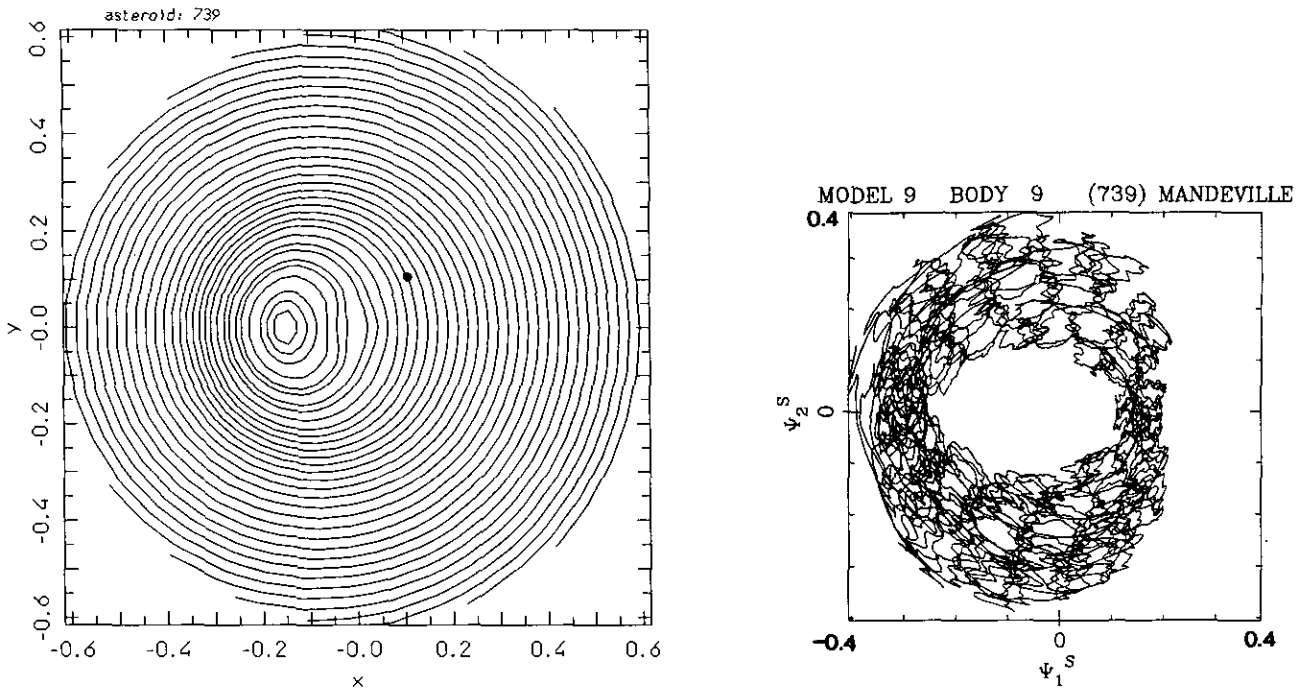

FIG. 4. Asteroid 739 Mandeville close to the ν_6 resonance.

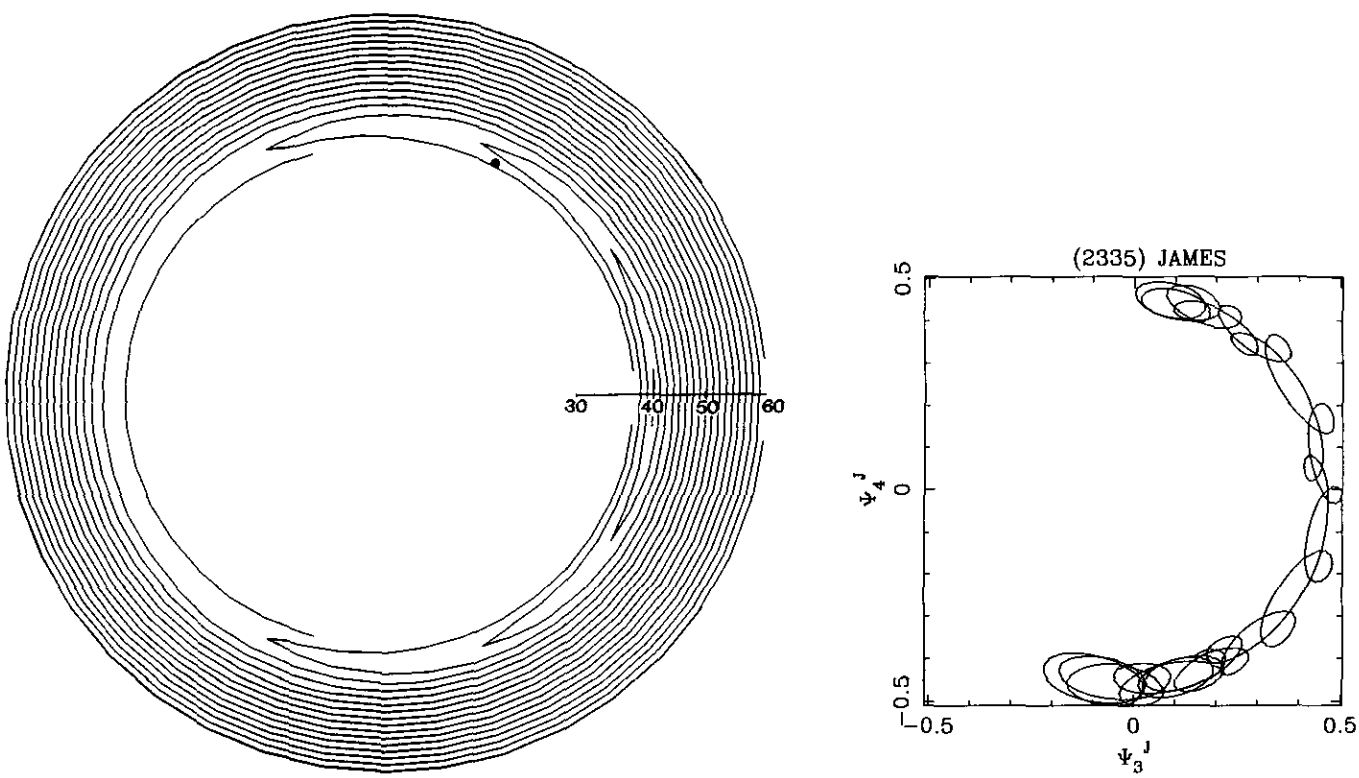

FIG. 5. Asteroid 2335 James, in the ν_{16} resonance and in the region of libration of the argument of perihelion ω.

Figure 4 refers to the asteroid 739 Mandeville. On the left I report the results provided by the resonant proper elements program; on the right the numerical integrations of Froeschlé and Scholl, plotted in the coordinates $\psi_1^S = [2(1 - \sqrt{1 - e^2})]^{1/2} \cos(\tilde{\omega} - \tilde{\omega}_S)$ and $\psi_2^S = [2(1 - \sqrt{1 - e^2})]^{1/2} \sin(\tilde{\omega} - \tilde{\omega}_S)$. Although the numerical simulation shows the superimposition of all secular modes, one can do a qualitative comparison with the theoretical result. Also in this case, it is possible to compute nonresonant proper elements, although with a poor accuracy; the nonresonant proper eccentricity turns out to be about 0.23 and should be interpreted qualitatively as the average of e over the circulation of σ. The behavior of 631 Philippina, also integrated in Froeschlé and Scholl (1987), is very similar to that of Mandeville.

The final case I analyze in this section is 2335 James. This asteroid, probably the nicest one from the dynamic point of view, is presently in a double resonance: the argument of perihelion librates around 90°, and the node librates around that of Jupiter in the ν_{16} resonance. The perturbation approach followed in Section 2 allows one to compute also the dynamic behavior of objects the argument of perihelion of which is in libration. On the left of Fig. 5 I show the results of my program on James. The coordinates are polar ones: the radius is the inclination; the angle is the critical one for the ν_{16} resonance; i.e., $\Omega - s_6 t - \mu_6^0$, or, equivalently, $\Omega - \Omega_J$. Curves are plotted only in the region of libration of the argument of perihelion ω and are cut when they encounter the Kozai critical curve which separates the ω-libration region from the ω-circulation region. Superimposed, I plot a scale for the inclination, ranging from 30 to 60°. James appears evidently in the banana-shape libration region of the ν_{16} resonance. On the right of Fig. 5 the results of the numerical simulation taken from Froeschlé *et al.* (1991) are shown. The coordinates are $\psi_3^J = [2(1 - e^2)^{1/2}(1 - \cos i)]^{1/2} \cos(\Omega - \Omega_J)$, $\psi_3^J = [2(1 - e^2)^{1/2}(1 - \cos i)]^{1/2} \cos(\Omega - \Omega_J)$. The integration confirms the banana-shape libration of James predicted by the model.

4. SYSTEMATIC EXPLORATION OF THE ν_6 RESONANCE

Many numerical simulations of fictitious objects in the asteroid belt show that the ν_6 resonance is able to pump up the eccentricity up to very large values (~0.8), unlike all other secular resonances (see Froeschlé and Scholl, 1992). This fact suggests that the ν_6 resonance is an active mechanism for the transport of objects to the inner Solar System. On the contrary, the previous examples of real asteroids lying in the ν_6 resonance show that the phase space can also be very regular and the evolution of the eccentricity bounded to moderate values. Therefore, this section is devoted to a systematic exploration of the ν_6 resonance in order to understand better its associated dynamic phenomena.

The ν_6 resonance has an unusual topology in the sense that the resonant phase space is different from the typical one described by the second fundamental model of resonance (Henrard and Lemaitre, 1983). In the second fundamental model one assumes that the Hamiltonian of the resonance has the form $H_0(S) + \varepsilon H_1(S) \cos\sigma$, with S, σ conjugated variables, and ε small. This assumption is satisfied in principle by secular resonances, ε being of order of e' or i'; however, the ν_6 resonance is particular, at least in the inner part of the asteroid belt ($a < 2.5$ AU), since H_0 is unusually small, of the same order of εH_1. An example is provided by Figs. 6 and 7, which show the energy profiles of the resonance for the two phase spaces illustrated later in Figs. 9 and 11. In Figs. 6 and 7 $x = e \cos\sigma$ ($\sigma = 0, \pi$); the dashed curve is the value of $H_0(e)$, i.e., $K_0(S, \Theta) + \nu S$ in formula (5), the dotted curve is $\varepsilon H_1(e) \cos\sigma$, i.e., $\alpha(S, \Theta) \cos\sigma$ in formula (5), and the solid curve is their sum H. As one sees, H_0 and εH_1 are of the same size, so that the profile of H has a very unusual shape compared with the typical one (see Ferraz-Mello, 1989).

The fact that H_0 is unusually small can be understood in a qualitative way looking at Fig. 8, taken from Morbidelli and Henrard (1991a) (similar to that in Williams and Faulkner, 1981), on the location of the ν_6

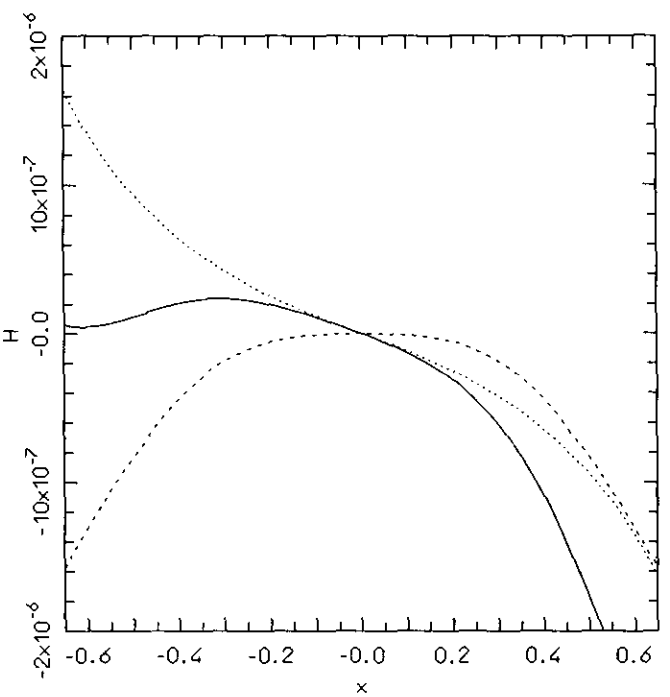

FIG. 6. The energy profiles of the phase space of Fig. 9 on the x axis. The dashed line is H_0, the dotted line is εH_1, and the solid line is $H = H_0 + \varepsilon H_1$. See text for further explanation.

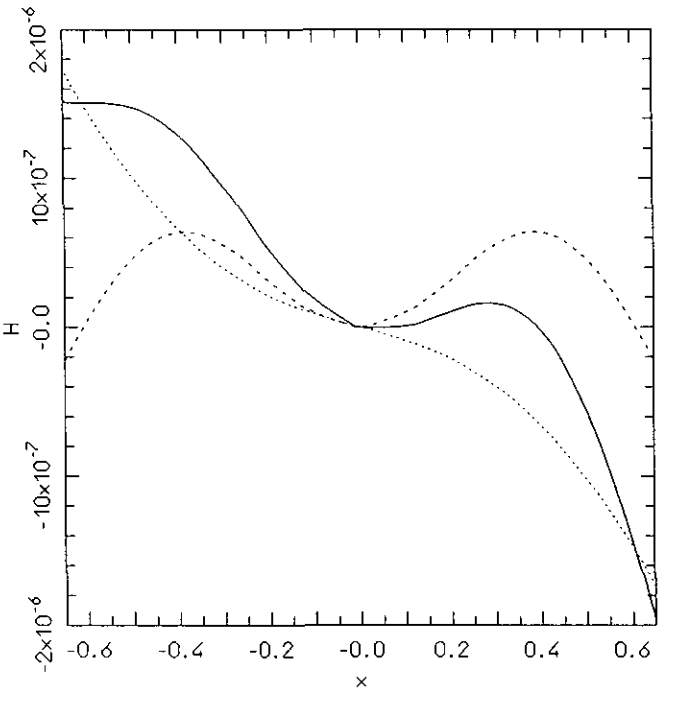

FIG. 7. The same as Fig. 6 for the phase space of Fig. 11.

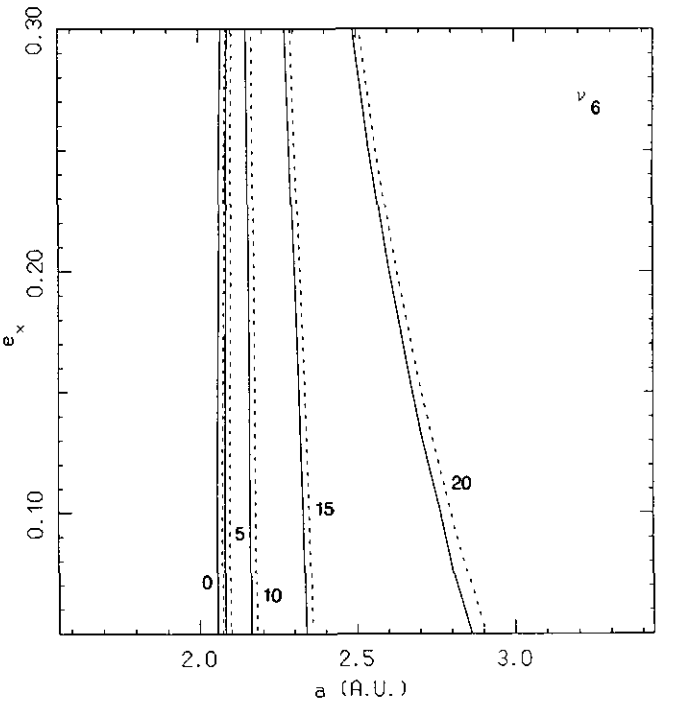

FIG. 8. The location of the ν_6 resonance in the a–e space for different values of the inclination.

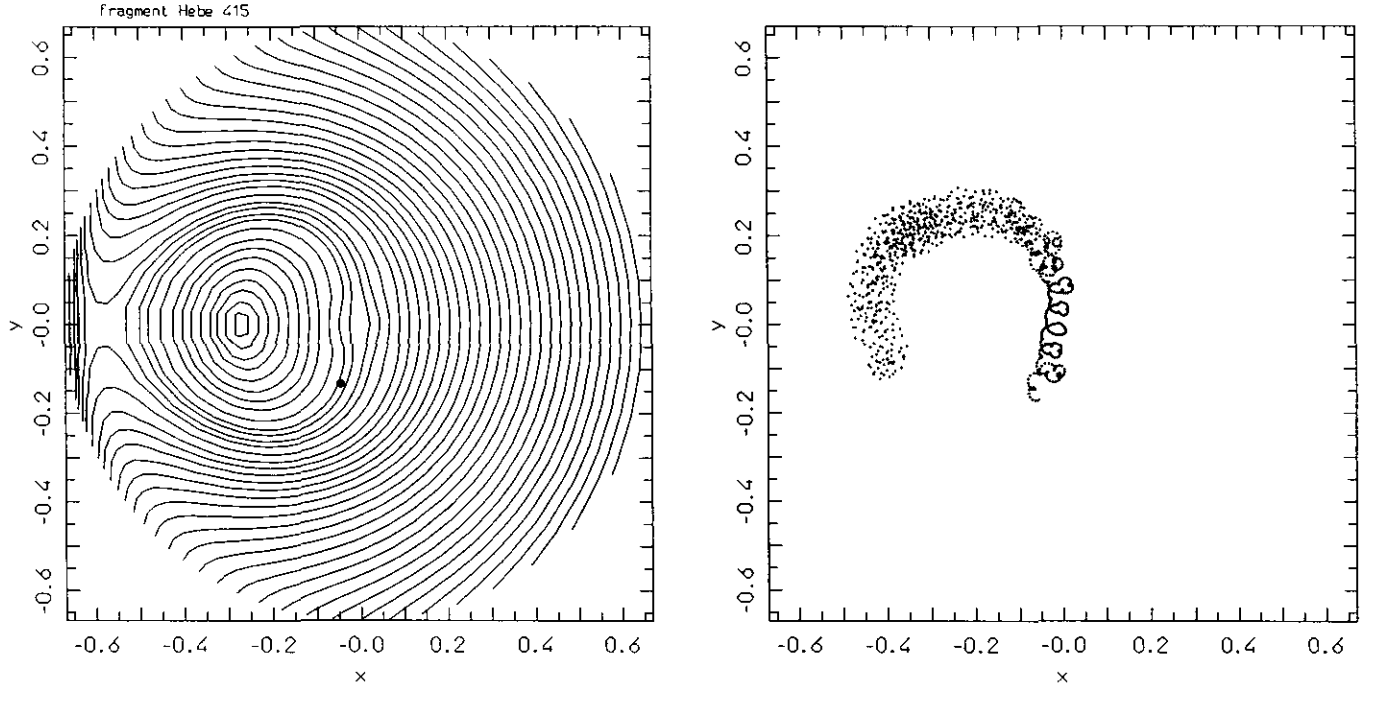

FIG. 9. Fictitious fragment of 6 Hebe. Initial conditions are: a = 2.3488 AU, e = 0.1802, i = 15.105°, ω = 242.81°, Ω = 138.750°, M = 328.350°.

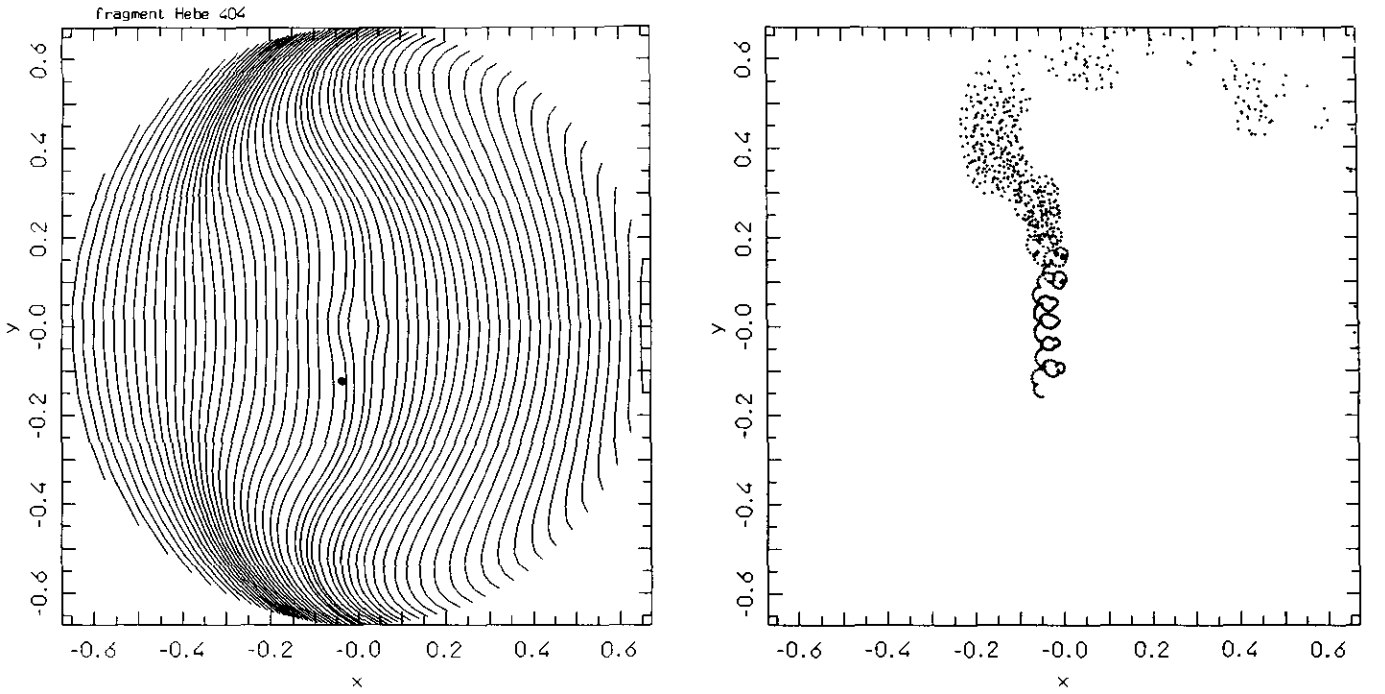

FIG. 10. Fictitious fragment of 6 Hebe. Initial conditions are: $a = 2.3051$ AU, $e = 0.1645$, $i = 14.474°$, $\omega = 245.77°$, $\Omega = 137.438°$, $M = 339.170°$.

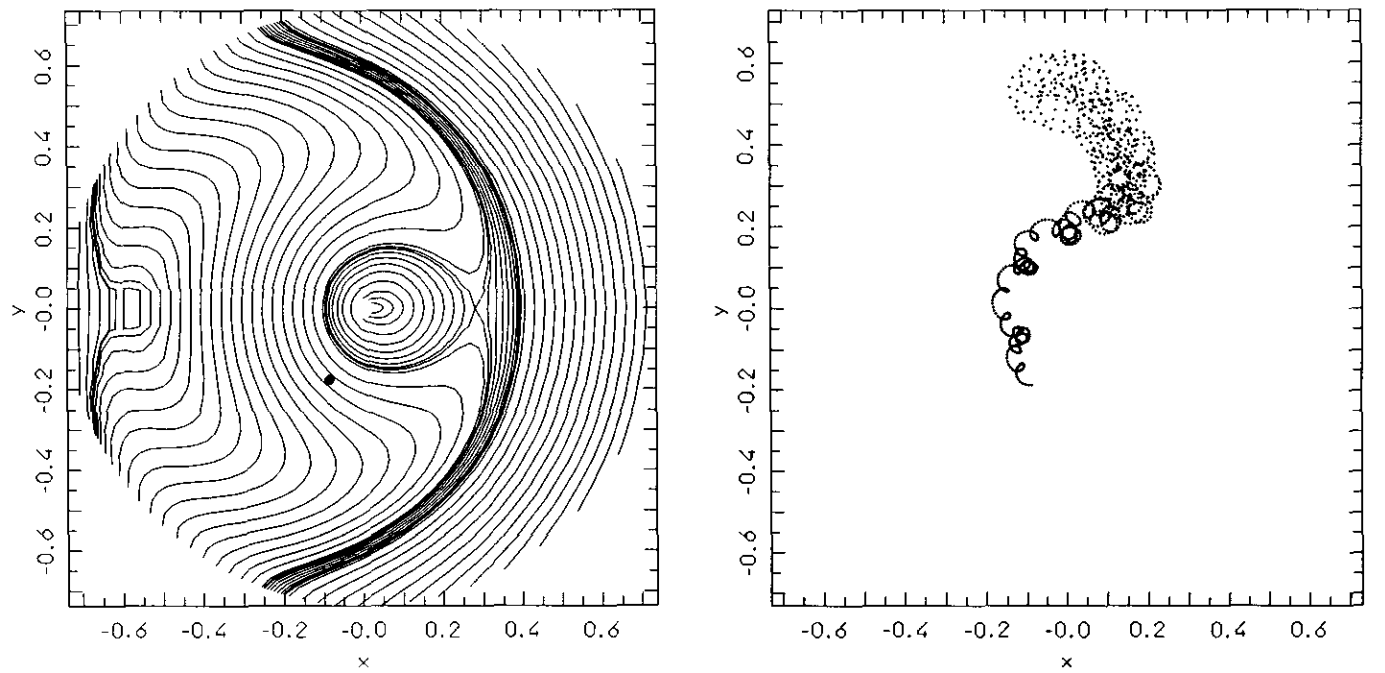

FIG. 11. Fictitious Hebe-like asteroid: initial conditions are those of Hebe, except the inclination, which is increased to 18.7°.

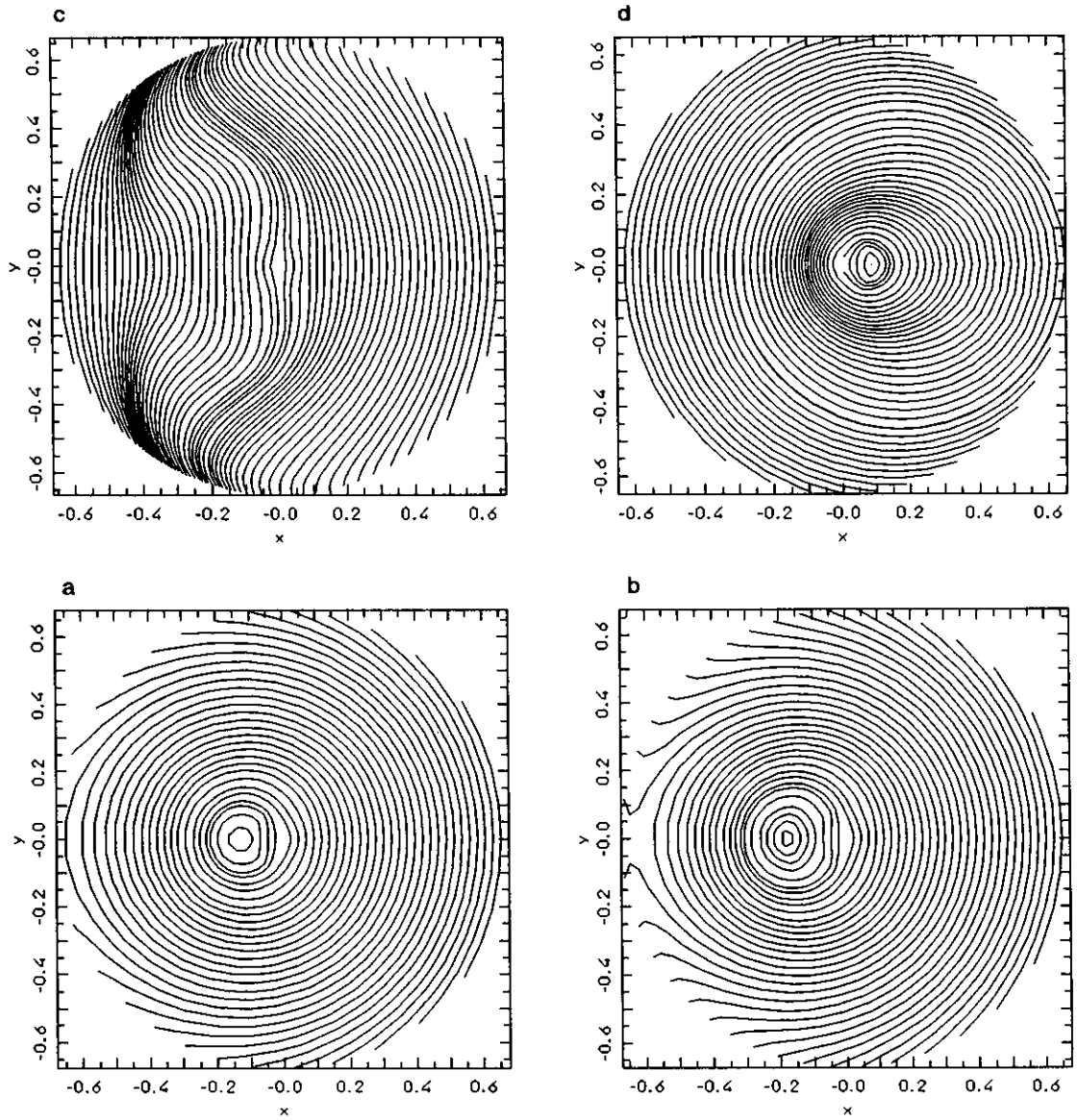

FIG. 12. Four resonant phase spaces at $a = 2.3488$ AU. All pictures refer to fictitious asteroids which have the same elements of the one in Fig. 9, but different values of the inclination: (a) $i = 14.105°$; (b) $i = 14.605°$; (c) $i = 15.605°$; (d) $i = 17.105°$.

resonance on the a–e plane for different values of the inclination. The striking feature is that, at least in the inner asteroid belt, the location of the ν_6 resonance is described by almost vertical lines, specifically, for given inclination and semimajor axis, the resonance occurs at *all* values of the eccentricity. Now, on a surface $\Theta \equiv J =$ constant, on which the resonant dynamics are confined, the inclination is almost constant; therefore $\partial H_0/\partial S = \dot{\sigma}$ is almost zero for all eccentricities. This explains why, in Figs. 6 and 7, H_0 does not change more than 10^{-6} in the range $-0.65 < x < 0.65$): the same order as εH_1.

As a consequence of these facts, the phase space of the ν_6 resonance can be quite "exotic," forcing the eccentricity of the asteroid to become very large; some examples are provided in Figs. 9, 10, 11. Figures 9 and 10 are computed for two fictitious fragments of the asteroid 6 Hebe which have been numerically integrated by Farinella *et al.* (1993). Their initial conditions are reported in the figure captions. The pictures on the left show the global aspect of the phase space in the usual coordinates x and y, the dots denoting the initial states of the fragments in the semiproper elements space. The pictures on the right show the results of the numerical integrations, in the same

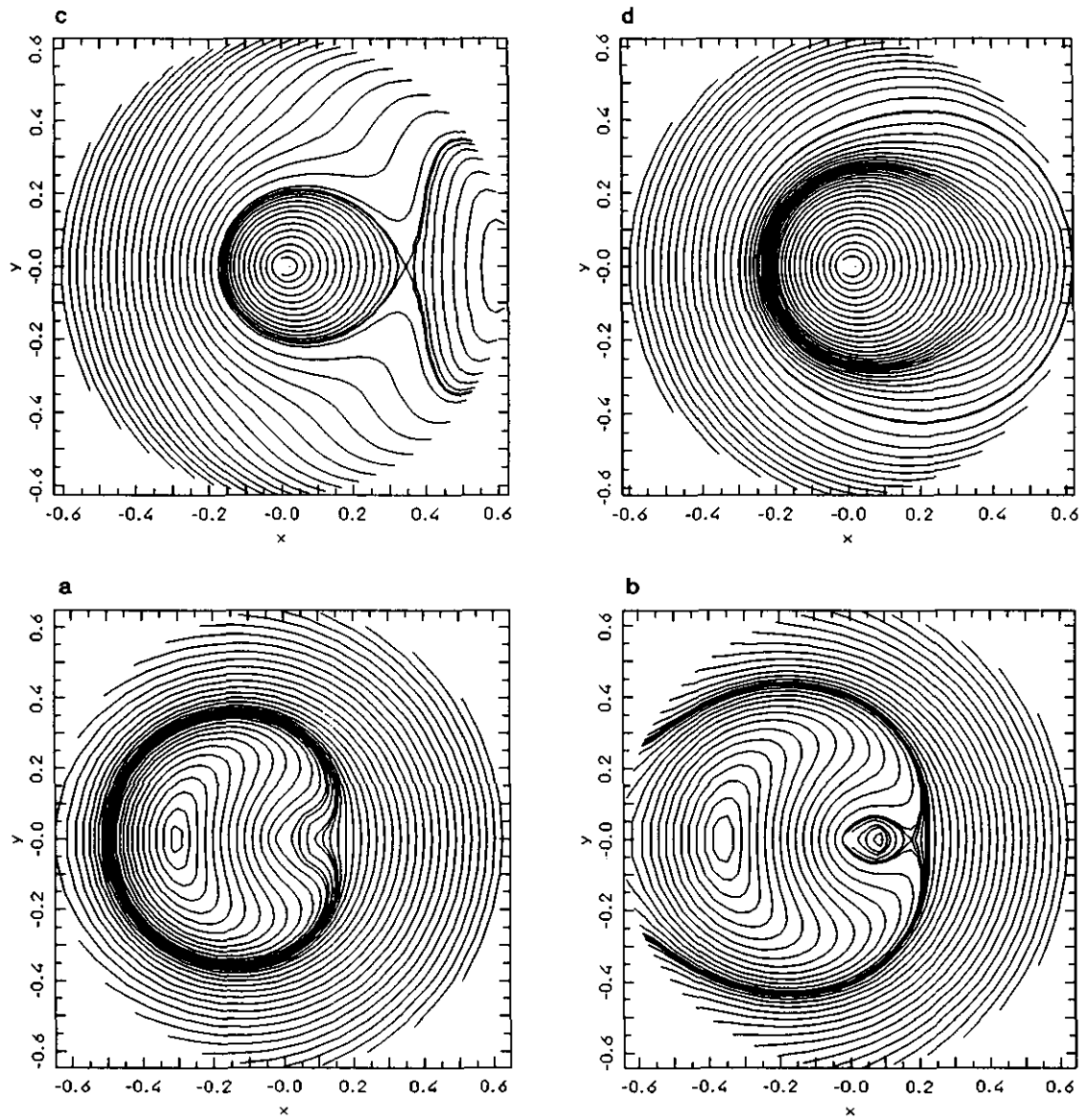

FIG. 13. Four resonant phase spaces at $a = 2.4253$ AU. All pictures refer to fictitious asteroids which have the same elements of 6 Hebe, but different values of the inclination: (a) $i = 17.7°$; (b) $i = 18.2°$; (c) $i = 19.7°$; (d) $i = 20.2°$. See also Fig. 11.

coordinates, up to the time when strong close encounters with Mars and the Earth start to happen. Figure 11 concerns a fictitious asteroid which has the same osculating elements as 6 Hebe but with the inclination increased to 18.7 degrees (for Hebe i is 14.7°); two unstable equilibrium points are visible in the picture! (The one at $\sigma = 180°$ could be an artifact of the model, which does not take into account the secular effects of the inner planets). The picture on the right of Fig. 11 shows the numerical simulation of this fictitious object up to the occurrence of strong close encounters with Mars. In the three cases, the numerical integrations match with the corresponding theoretically computed phase space, proving that these exotic pictures of the phase space describe properly the ν_6 dynamics, at least at moderate eccentricities.

Some more details must be added on the comparisons with the numerical integrations in this section. First of all I changed the value of the secular frequency g_6 (usually that given in Nobili *et al.*, 1989) accordingly to the value resulting from the numerical integrations, which is different from the real one because Uranus and Neptune were not included. Second, I increased the frequency of σ given by my model of 0.4 arsec/year. This empirical correction of the theoretical results has turned out to be necessary

in order to match *all* the numerical integrations of objects lying deeply inside the ν_6 resonance (for objects relatively far from critical curves like Vinifera and Mandeville this correction has no appreciable effect). The necessity of an empirical correction should not be surprising. All models are simplified and have some systematic error, due to the fact that some perturbations are neglected or considered in an approximate fashion. In this case, for example, I neglect the direct effect of the inner planets (which are taken into account in the numerical simulations) and the terms proportional to the square of Jupiter's eccentricity and inclination. As a matter of fact, the contribution of these neglected perturbations to the final frequency of σ can be estimated to be just of the order of my "empirical correction" in the neighborhood of the ν_6 resonance.

At this point, I am ready to make a systematic exploration of the ν_6 resonance. Figures 12 and 13 show the topology of the phase space on surfaces $\Theta \equiv J$ = constant, for a = 2.349 AU and a = 2.425 AU, respectively. Essentially, the inclination increases from picture (a) to picture (d), therefore passing from "below" the resonance to "above" the resonance. It is important to observe that the unstable equilibrium point is at σ = 180° when a = 2.349 AU, while it is at σ = 0° when a = 2.425 AU. The reason of this basic change in the resonant structure of the phase space should be looked for in the different relative sizes of H_0 and εH_1, as shown in Figs. 6 and 7. The topology of the phase space changes again in correspondence with the 3/1 mean-motion commensurability: for a in between 2.5 and 2.7 AU, the unstable equilibrium point is again at σ = 0 (see Fig. 3 in Morbidelli and Henrard, 1981b). A new change occurs further away, since in between 2.7 and 2.8 AU the resonant structure of the phase space is again similar to that in Fig. 13. R. Gonczi has kindly made many numerical simulations (apart from those shown here) in order to test these results of the resonant proper elements program. The agreement between the numerical integrations and theoretical model is always good. The only cases of evident inconsistency have been found for fictitious objects lying in mean motion resonances even of high order, like 11/4 or 8/3. This is not surprising, since the double average of the Hamiltonian with respect to the mean anomalies is at the base of the construction of my analytical model of secular dynamics.

Figure 14 points out which are the dangerous regions of the ν_6 resonance, i.e., the sets of the initial conditions which lead to large eccentricity. The initial conditions are in the space of mean elements. The eccentricity is assumed to be equal to 0.15; the semimajor axis is chosen on a grid ranging from 2 to 2.8 AU with a stepsize of 0.025 AU; the inclination has a stepsize of 1°. For what concerns the angles, I choose four values of ω and Ω. Figure 14a is made for ω = 0° and Ω = 124.19° (σ = 0°);

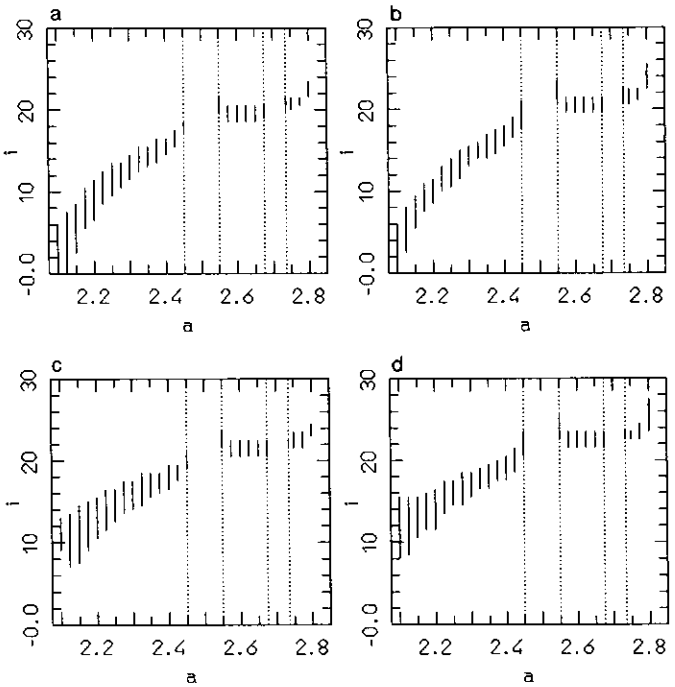

FIG. 14. The sets of the initial conditions in the ν_6 resonance, which lead to $e > 0.4$.

Fig. 14b is for ω = 180° and Ω = 124.19° (σ = 180°); Fig. 14c is for ω = 180° and Ω = 304.19° (σ = 0°); Fig. 14d is for ω = 0° and Ω = 304.19° (σ = 180°). The dashed region denotes the sets of initial conditions which lead to $e > 0.4$; the two gaps around 2.5 and 2.7 AU are due to the presence of the 3/1 and 8/3 resonances, in the vicinity of which the averaged theory does not work. The 8/3 is a faint resonance, but, being located at 2.70 AU, is detected by the grid of initial conditions; conversely, other resonances like the 7/2 are not detected by my grid. Their dynamic effect, however, is taken into account through the computation of the quadratic term in the masses. The fact that the location of the dangerous region changes quite significantly is Figs. 14c and 14d with respect to 14a and 14b is due to the initial phase of the node, which acts on the inclination, especially in the inner belt, near to the ν_{16} resonance. All computations have been made by applying the empirical correction of 0.4 arsec/year.

Finally, I analyze by the resonant proper elements program a list of 46 numbered asteroids selected with the following criteria: (1) their perihelion distance is larger than 1.1 AU; (2) they are close to the ν_6 resonance, so nonresonant proper elements cannot be provided or have a poor accuracy. From the dynamic point of view, these are among the best candidates to become Earth crossers in the set of all numbered asteroids with current moderate

TABLE I

Mean Elements of the Asteroids Close to the ν_6 Resonance Analyzed in This Paper

No.	ω	Ω	i	e	a	No.	ω	Ω	i	e	a
6	235.3	138.9	13.438	0.202	2.4253	2038	186.1	66.5	13.510	0.090	2.43520
31	67.1	24.4	26.008	0.222	3.1530	2064	5.3	295.6	7.236	0.329	2.17819
234	187.7	144.9	14.135	0.244	2.3857	2368	42.2	284.2	6.826	0.412	2.10536
413	252.0	100.5	17.187	0.343	2.5830	2380	124.9	304.6	3.321	0.059	2.19194
426	222.0	306.6	20.966	0.104	2.8885	2548	291.7	295.4	19.698	0.101	2.63317
512	248.8	103.7	7.174	0.253	2.1895	2604	132.4	121.5	13.320	0.232	2.38790
623	126.9	303.0	15.654	0.113	2.4603	2642	158.6	203.8	14.674	0.184	2.42605
739	41.6	135.6	19.330	0.142	2.7376	2645	85.0	341.1	14.588	0.106	2.39138
759	2.8	313.0	21.304	0.206	2.6176	3050	58.4	262.8	2.644	0.188	2.22488
930	333.8	333.3	16.304	0.144	2.4310	3102	143.7	179.2	7.865	0.448	2.15157
1022	124.8	109.2	19.530	0.170	2.8077	3356	156.8	105.4	2.516	0.113	2.19285
1159	318.6	339.0	13.888	0.058	2.3796	3402	318.6	339.2	5.578	0.279	2.13181
1182	69.1	326.6	10.499	0.117	2.25956	3558	309.1	336.3	14.300	0.066	2.44138
1222	55.6	245.7	20.884	0.250	2.79135	3665	278.7	112.8	13.492	0.088	2.41829
1468	25.5	302.7	11.433	0.270	2.19577	3833	166.5	173.8	11.355	0.388	2.19571
1492	71.3	144.0	4.759	0.116	2.17308	3858	344.0	335.5	8.595	0.242	2.18949
1629	101.6	134.0	8.299	0.154	2.23821	3939	254.9	26.0	24.405	0.095	3.11376
1706	335.0	280.0	3.445	0.114	2.12550	4002	193.6	114.9	13.221	0.027	2.51555
1739	57.9	223.8	3.898	0.123	2.26114	4095	77.1	264.7	3.947	0.118	2.12014
1892	95.6	309.7	15.394	0.089	2.46170	4320	263.1	201.7	6.460	0.113	2.19688
1916	340.6	332.2	13.848	0.449	2.27276	4547	41.8	350.6	18.598	0.068	2.61353
2015	279.7	335.4	12.835	0.104	2.33541	4770	199.9	127.5	23.650	0.303	2.86497
2033	139.4	313.2	9.809	0.111	2.22539	4923	94.3	198.8	6.610	0.201	2.14491

eccentricity. The list of the mean elements of these asteroids as provided by Milani and Kneževičis reported in Table I.

For only two of these asteroids, i.e., 1706 Dieckvoss and 2380 Heilongjiang, the algorithm for the computation of semiproper elements does not converge, since the inclination and the eccentricity are both small ($i = 0$ and $e = 0$ are both singularities for the action-angle variables used here, as explained in Section 2); for all the others, resonant proper elements can be computed and are reported in Table II. For the same reason (small initial eccentricity and inclination) the resonant proper elements of 1739, 3050, 3356, and 4095 are somewhat poor, but not enough to put in doubt their dynamic stability. Table II gives

TABLE II
Numbered Asteroids Close to the ν_6 Resonance

No.	a	σ	e	$T(10^3\text{y})$	No.	a	σ	e	$T(10^3\text{y})$
6	2.425	0	0.08	107	31	3.153	0	0.21	73
		180	0.26	316			180	0.38	398
234	2.386	0	0.08	187	413	2.583	0	0.13	163
		180	0.27	430			180	0.37	400
426	2.889	180	0.27	106	512	2.190	0	0.03	202
		0	0.15	230			180	0.33	623
623	2.460	0	0.09	33	739	2.738	180	0.40	199
		180	0.23	190			0	0.17	443
759	2.618	180	0.14	271	930	2.431	180	0.14	271
		180	0.26	610			180	0.17	524
1022	2.808	180	0.29	53	1159	2.380	180	0.13	196
		0	0.06	211			180	0.05	399
1182	2.260	0	0.04	54	1222	2.791	180	0.29	30
		180	0.20	249			180	0.18	280
1468	2.196	180	0.11	386	1492	2.173	180	0.30	230
		143	0.60	2080			0	0.05	542
1629	2.238	180	0.28	167	1739	2.261	180	0.13	18
		0	0.06	447			0	0.07	128
1892	2.462	0	0.03	68	1916	2.273	0	0.25	227
		180	0.20	288			180	0.46	472
2015	2.335	180	0.17	99	2033	2.225	0	0.10	18
		0	0.01	330			180	0.26	237

for each asteroid its number, its semimajor axis, and the configuration angle, eccentricity, and time (in thousands of years starting from the present epoch) corresponding to two successive passages through the axis $\sigma = 0$, $\sigma = 180$. This allows one to understand completely the dynamic behavior of the asteroid; for example, σ is 6 Hebe circulates, while in 759 Vinifera librates around 180°. Conversely, if the asteroid's eccentricity increases up to more than 0.6, and therefore is such that my model (which does not take into account the perturbations of the inner planets) is no longer accurate, Table II gives the final angle, eccentricity, and time (this occurs for example for 2368 Beltrovata). In Table II, the eccentricity is computed on the section $\omega = 90°$ and therefore is the largest one assumed during the circulation of ω. Table II shows that most of these asteroids, like 6 Hebe, are outside the dangerous regions of the ν_6 resonance and have a moderate eccentricity along all their secular evolution. Some of them, although regular from the point of view of resonant dynamics, become temporary Mars crossers. Only four

TABLE II—*Continued*

No.	a	σ	e	$T(10^3 y)$	No.	a	σ	e	$T(10^3 y)$
2038	2.435	180	0.17	97	2064	2.178	180	0.33	7
		0	0.02	325			0	0.14	257
2368	2.105	180	0.35	170	2548	2.633	180	0.30	200
		130	0.60	585			0	0.01	537
2604	2.388	180	0.31	90	2642	2.426	0	0.07	113
		0	0.10	345			180	0.24	318
2645	2.391	0	0.06	35	3050	2.225	0	0.09	110
		180	0.24	259			180	0.18	237
3102	2.152	180	0.08	672	3356	2.193	180	0.15	68
		137	0.60	1601			0	0.05	259
3402	2.132	180	0.28	41	3558	2.441	180	0.11	147
		180	0.08	421			180	0.05	347
3665	2.418	0	0.02	85	3833	2.196	180	0.11	461
		180	0.25	406			124	0.60	1161
3858	2.189	0	0.05	231	3939	3.114	180	0.25	227
		180	0.24	507			180	0.10	510
4002	2.516	180	0.19	41	4095	2.120	0	0.01	323
		180	0.05	83			180	0.21	944
4320	2.197	0	0.10	12	4547	2.614	0	0.01	53
		180	0.28	251			180	0.18	250
4770	2.865	0	0.18	167	4923	2.145	180	0.31	864
		180	0.39	352			180	0.17	1932

of them are forced to very large eccentricity ($e > 0.6$) and can become Earth crossers: these are 2368 Beltrovata and 3102 (1981 QA) (already classified in the "Eros" class by Milani *et al.*, 1989), 1468 Zomba, and 3833 1971 SC. Figure 15 shows the evolution of the eccentricity of 2368 Beltrovata, integrated in (Froeschlé and Scholl, 1987): indeed the eccentricity grows up to cometary values, as predicted. I stress, however, that some asteroids could avoid such a catastrophic evolution, owing to close encounters. An example is provided by Gonczi's numerical integration of asteroid 3102, which is shown in Fig. 16. In this case, a very close encounter with Mars (4.8×10^{-4} AU) changes abruptly the semimajor axis, putting the asteroid in a safer region of the ν_6 resonance; this stops the secular growth of the eccentricity. As a matter of fact, since the model does not include the inner planets, the results of Table II can only indicate whether the conditions for close encounters will be fulfilled. A final remark concerns 1468 Zomba. According to my computations, (see Fig. 17, on the left), this asteroid is very close to the separatrix, and its eccentricity should increase up to 0.6 in 2 Myr, after having spent most of the time near the saddle point. For evident

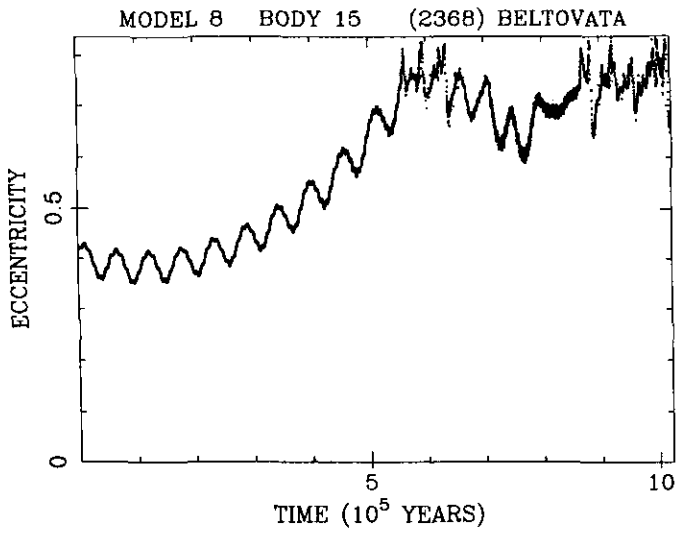

FIG. 15. The evolution of the eccentricity of 2368 Beltrovata as found in Froeschlé and Scholl (1987).

reasons, this result is very sensitive to any possible error; for example, by changing the frequency of 0.1 arsec/year the phase space becomes that shown in the picture on the right of Fig. 17, with the asteroid safe in the island of libration around 180°. Therefore, much care should be taken in integrating numerically the orbit of this asteroid.

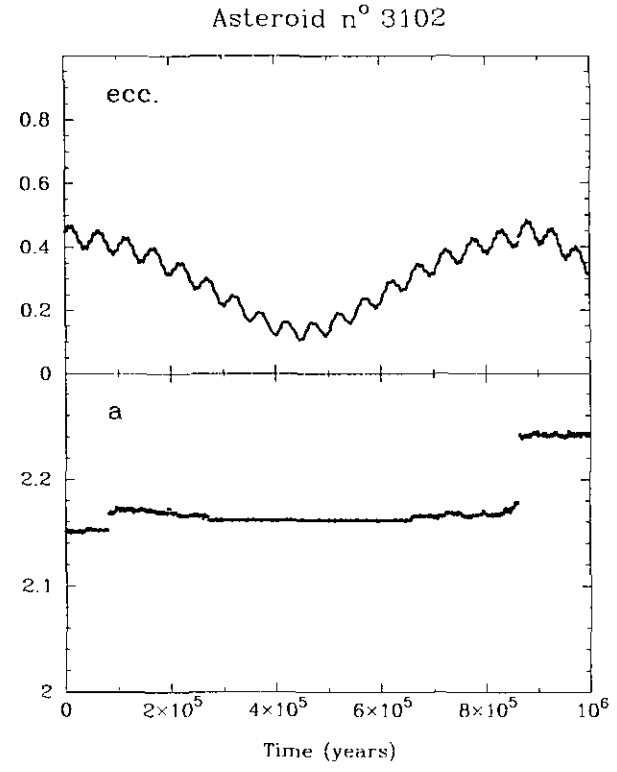

FIG. 16. Numerical integration of 3102 (1981 QA) by R. Gonczi. (Top) The evolution of the semimajor axis. (Bottom) The evolution of the eccentricity. A very close encounter with Mars puts the asteroid in a safe region of the ν_6 resonance where the critical argument circulates. As a consequence the growth of the eccentricity stops.

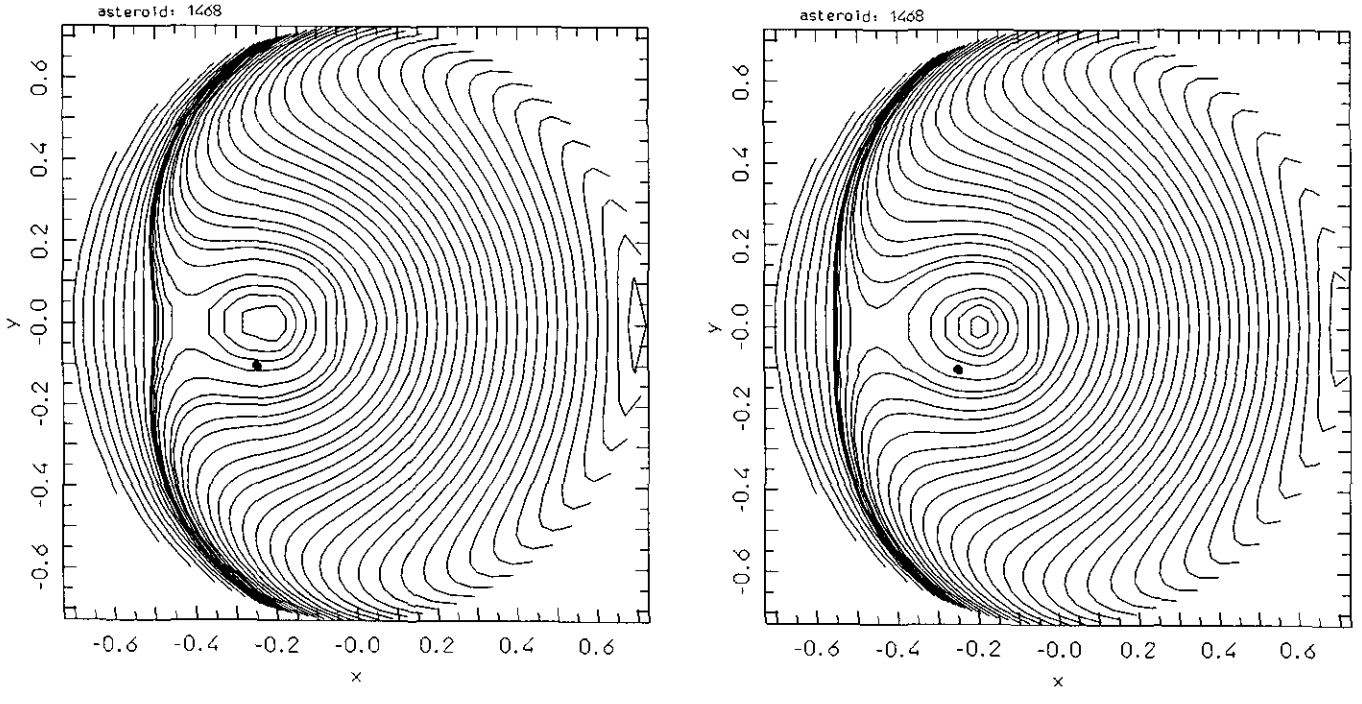

FIG. 17. The phase space around 1468 Zomba. On the left the results of the model, which predicts that the eccentricity of Zomba will grow up to 0.6 in 2 Myr (see also Table II). However, a small perturbation of the model, e.g., changing the g_6 frequency by 0.1 arsec/year, provides a qualitatively different result shown on the right.

5. CONCLUSIONS

The resonant proper elements algorithm allows one to compute the dynamic evolution of objects close to a secular resonance. The comparisons with the numerical integrations show that the results are fairly accurate, enough to achieve the goal of the algorithm, which is to identify the dynamic nature of resonant objects, i.e., to distinguish among librators and circulators, future planet crossers, and regular bodies. The short CPU time necessary for its execution makes the algorithm a useful tool for the analysis of thousands of fictitious objects, in order to carry out a systematic exploration of the dynamics of asteroid fragments, to be applied in particular to the problem of meteorite transport. This will be done in a forthcoming paper. We also plan to study in a more detailed way all the real asteroids (including the planet crossers) which are inside the main secular resonances.

ACKNOWLEDGMENTS

I particularly thank Robert Gonczi for the many numerical integrations he has made in order to test my theoretical work, always with the kindness which distinguishes him. I am grateful also to Christiane Froeschlé and Paolo Farinella, whose "resonant nose" guided me in this work with many precious suggestions.

REFERENCES

FARINELLA, P., CH. FROESCHLÉ AND R. GONCZI 1993. Meteorites from the asteroid 6 Hebe *Celest. Mech.*, **56,** 287–305.

FERRAZ-MELLO, S. 1989. Averaging Hamiltonian systems. In *Modern Methods in Celestial Mechanics* (D. Benest and C. Froeschlé, Eds.). Editions Frontières.

FROESCHLÉ, CH., AND H. SCHOLL 1987. Orbital evolution of asteroids near the secular resonance ν_6. *Astron. Astrophys.* **179,** 294–303.

FROESCHLÉ, CH., A. MORBIDELLI, AND H. SCHOLL 1991. Complex dynamical behaviour of the asteroid 2335 James associated with the secular resonances ν_5 and ν_{16}: Numerical studies and theoretical interpretation. *Astron. Astrophys.* **24,** 553.

FROESCHLÉ, CH., AND H. SCHOLL 1992. The effect of secular resonances in the asteroid region between 2.1 and 2.4 A.U. In *Asteroids, Comets, Meteors 1991*, pp. 205–209. Lunary and Planetary Institute, Houston.

HENRARD, J., AND A. LEMAÎTRE 1983. A second fundamental model for resonance. *Celest. Mech.* **30,** 197–218.

KOZAI, Y. 1962. Secular perturbations of asteroids with high inclination and eccentricities. *Astron. J.* **67,** 591–598.

LEMAÎTRE, A., AND A. MORBIDELLI 1992. Computation of proper elements for high inclined asteroids. Submitted for publication.

MILANI, A., M. CARPINO, G. HAHN, AND A. NOBILI 1989. Dynamics of planet-crossing asteroids: Classes of orbital behavior. Project SPACEGUARD. *Icarus* **78,** 212–269.

MILANI, A., AND Z. KNEŽEVIĆ 1990. Secular perturbation theory and computation of asteroid proper elements. *Celest. Mech.* **49,** 247–411.

MILANI, A., AND Z. KNEŽEVIĆ 1992. Asteroid proper elements and secular resonances. *Icarus* **98,** 211–232.

MORBIDELLI, A., AND J. HENRARD 1991a. Secular resonances in the asteroid belt: Theoretical perturbation approach and the problem of their location. *Celest. Mech.* **51,** 131–167.

MORBIDELLI, A., AND J. HENRARD, 1991b. The main secular resonances ν_6, ν_5 and ν_{16} in the asteroid belt. *Celest. Mech.* **51,** 169–197.

NAKAI, H., AND H. KINOSHITA 1985. Secular perturbations of asteroids in secular resonances. *Celest. Mech.* **36,** 391–407.

NOBILI, A., A. MILANI, AND M. CARPINO 1989. Fundamental frequencies and small divisors in the orbits of the outer planets. *Astron. Astrophys.* **210,** 313–336.

SCHOLL, H., AND CH. FROESCHLÉ 1990. Orbital evolution of known asteroids in the ν_5 resonance region. *Astron. Astrophys.* **227,** 255–263.

WILLIAMS, J. G. 1969. *Secular Perturbations in the Solar System*. Ph.D. dissertation, University of California, Los Angeles.

WILLIAMS, J. G., AND J. FAULKNER 1981. The position of secular resonance surfaces. *Icarus* **46,** 390–399.

YOSHIKAWA, M. 1987. A simple analytical model for the ν_6 resonance. *Celest. Mech.* **40,** 233–272.